A Dynamically Consistent, Multi-Variable Ocean Climatology

Ichiro Fukumori*, Patrick Heimbach †, Rui M. Ponte‡ and Carl Wunsch§ ¶

*Jet Propulsion Laboratory, Pasadena, CA

†University of Texas at Austin, Austin Texas

‡Atmospheric and Environmental Research, Inc., Lexington, Massachusetts

§*Corresponding author address:* Carl Wunsch

E-mail: carl.wunsch@gmail.com

¶Massachusetts Institute of Technology and Harvard University, Cambridge Massachusetts

ABSTRACT

A dynamically consistent 20-year average ocean climatology based on monthly values during the years 1994-2013 has been produced from the most recent state estimate of the Estimating the Circulation and Climate of the Ocean (ECCO) project, globally, top-to-bottom. The estimate was produced from a least-squares fit of a free running ocean general circulation model to almost all available near-global data. Data coverage in space and time during this period is far more homogeneous than in any earlier interval and includes CTD, elephant seal, and Argo temperature and salinity profiles, sea-ice coverage, the full altimetric and gravity-field coverage, satellite sea-surface temperatures, as well as the initializing meteorological coverage from the ECMWF ERA-Interim reanalysis. Dominant remaining data inhomogeneity arises from the increasing coverage from the Argo profiles beginning about 2000 to present. The state estimate exactly satisfies the free running MITgcm at all times and hence produces values satisfying the fundamental conservation laws of energy, freshwater etc., permitting its use for climate change studies. Quantities such as calculated heat content depend upon all observations, not just temperature, e.g. altimetric height and meteorogical exchanges. Output files are publicly available in netCDF and .mat form and include hydrographic variables, three components of velocity, and pressure as well as other variables including inferred air-sea momentum and buoyancy fluxes, 3D mixing parameters, and sea-ice cover. (Capsule Summary) A 20-year ocean climatology is available that includes all dynamical variables and is consistent with a diversity of global data.

1. Introduction

Climatologies, defined as temporal averages of elements of the climate state, have been important in numerous studies. They serve as reference states for inferring changes, as initial conditions in forecasts, and sometimes as the basis of diagnostic dynamical calculations. In an oceanographic context, the most widely employed global climatology has probably been the hydrographic compilation produced initially by Levitus et al. (1982) and its successors as the World Ocean Atlas (WOA). They used data from the entire history of physical oceanographic measurements of temperature and salinity as a function of horizontal position and depth. Other global averages include that of Gouretski and Koltermann (2004), from data of the World Ocean Circulation Experiment. A number of climatologies of the upper ocean are based primarily on XBT data in the early years (e.g., Ishii et al. 2003; AchutaRao et al. 2007). In related work, but with different emphases, a number of studies of the changing ocean state have been undertaken extending back into the 19th Century (e.g., Kennedy et al. 2011).

A major issue with most such climatologies and studies based on them has been the very great inhomogeneity with which the ocean has been observed over the years (Fig. 1) and in which the filling of space and time gaps in the record has relied upon sometimes plausible, but generally untestable, statistical assumptions (see e.g., Boyer et al. 2016; Wunsch 2016). Only temperature, or in a few cases temperature and salinity, data were available. Furthermore, to our knowledge, no previous extended-time ocean climatology has comprised any variables except the hydrographic ones.

The World Ocean Circulation Experiment (WOCE) was designed in large-part to produce the first truly global, time-varying estimate of the circulation over approximately a decade, an estimate that would be useful in defining the major climatologically important ocean elements (see Siedler

et al. 2013). Until recently, even the best inverse calculations (e.g., Ganachaud and Wunsch 2003; Lumpkin and Speer 2007), were forced to treat quasi-synoptic sections distributed globally over decades as though they represented a consistent time-average or, paradoxically, as a snapshot. Such assumptions ultimately are not tenable in a rapidly varying oceanic flow. The Estimating the Circulation and Climate of the Ocean (ECCO) project was formed to address this goal using both the conventional and newly-deploying WOCE observation system, along with the rapidly advancing time-varying general circulation modelling capability (Stammer et al. 2002). This present paper is intended to introduce another climatology, based on an updated edition (Release 3; Fukumori et al. 2017) of the latest Version 4 of the ECCO ocean state estimate (Forget et al. 2015). The climatology here is focussed on the 20-year period 1994-2013, an interval in which a comparatively homogeneous set of global-scale observations were obtained so that the zero-order sampling difficulties visible in Fig. 1 are much reduced. The major inhomogeneity in the present climatology stems from the growing availability of Argo floats beginning about 2000 and extending to the present day (Roemmich et al. 2009), but the dominant data sets, including altimetry, CTDs, etc., are nearly homogeneous over the entire interval and, in particular, do not display the northern-southern hemisphere asymmetries plaguing earlier climatologies. Use of dynamics further reduces effects of remaining inhomogeneities.[1]

Atmospheric climatologies are sometimes defined as averages over 30-year intervals, a duration determined by the behavior of weather statistics. A comparable interval in the ocean would, because of the much longer time-scales involved, probably encompass hundreds of years, and even then statistical stability is not guaranteed. A 20-year ocean average does suppress much high frequency variability, and is a useful reference state.

[1]The estimation interval begins in 1992 and extends nearly to the present time. Data observed prior to 1992 appear only tangentially in constructing first-estimate adjustable initial conditions from previous climatologies.

Essentially all of the available hydrographic data are used, including CTD hydrography (Talley et al., 2016), measurements from elephant seals (Roquet et al. 2013), XBTs and Argo temperature and salinity profiles (Riser et al., 2016) as well as sea surface temperature products (Reynolds and Smith, 1994,1995). But *in addition,* the complete altimetric record, which begins in 1992, is employed (e.g., Fu and Cazenave 2001), as are the GRACE satellite gravity measurements (Quinn and Ponte 2008; Watkins et al. 2015), and the available a priori estimates of the meteorological forcing during the climatological interval (Dee et al. 2011, 2014). A nearly complete list is contained in Table 21.2 of Wunsch and Heimbach (2013) with details of about 11 generic data types. Fukumori et al. (2018) provide full details of data sources, processing and uncertainty weights.

Combining Data and Dynamics To combine the diverse data sets including the surface forcing fields, a least-squares fit was made of a state-of-the-art ocean/sea ice general circulation model (Forget et al. 2015; cf. Marshall et al. 1997; Adcroft et al. 2004; Wunsch and Heimbach 2007, 2013; and Wunsch et al. 2009). As is done in conventional least-squares fitting, all data are weighted by the best-available estimates of their uncertainties—written as error variances or covariances. Because of the huge dimension of the resulting calculation, the fit is carried out by numerical iteration using Lagrange multipliers (adjoint or dual solutions; see Wunsch and Heimbach 2013; Forget et al. 2015)). The Lagrange multipliers enforce the model, which includes numerous adjustable parameters.

The state estimate over the 20 years is obtained from the *free-running* ECCO configuration of the MITgcm, started from the adjusted initial conditions and mixing coefficients, and subject to the adjusted meteorological forcing fields. Time-step of the model is 1 hour over the interval 1992-2015 with only the shorter interval 1994-2013 used in the present climatology. As the product

of a GCM, one by construction generally reproducing within error estimates all of the data used, the state estimate includes values of the three-dimensional time-varying velocity field, the surface elevation and its changes, bottom pressure, ice-cover, as well as the parameters representing the non-resolved eddy-mixing via the bolus transport of Gent and McWilliams (1990) and related schemes. Also included are the misfit fields to the different data sets used as constraints. As fitting iterations continue, new data are added, the duration increases, and the model continues to develop, the climatology changes, although at this stage, future adjustments are expected to be quantitatively small in most aspects.

Differences from Existing Ocean Climatologies

In specific contrast to what are usually called "reanalysis products," the state estimate satisfies all of the conventional conservation requirements for any dynamically consistent climate component, including energy, heat, freshwater, vorticity—up to the accuracy of the general circulation model equations. Although considerable extra computation is required to obtain dynamically consistent solutions, no artificial interior sources and sinks appear (Wunsch and Heimbach 2013; Stammer et al. 2016) thus permitting study of changes in energy, heat-content, etc. The great power of diverse data sets is brought to bear on all of the elements of the state estimate. All observations have limits of sampling, random and bias errors, and finite duration. So for example, even the revolutionary Argo data sets fail to adequately depict important physical processes (e.g., Evans et al., 2017). The state estimate provides, in addition to the directly measured variables, all those required by or computable from a general circulation model.

2. Basic Fields

A description of the time-varying three-dimensional global oceanic state and its interpretation is a forbidding undertaking. What is intended here is to call attention to the availability of fields

useful for a great variety of purposes, explain how to obtain the fields in simple ways, and to invite the use and critique of the result by the wider community. A more elaborate pictorial description has been posted with links from the ECCO website, at the present moment in two distinct Parts. Part 1 (ECCO Consortium 2017a) is devoted to the hydrographic and derived fields such as surface elevation and mixed-layer depths. Part 2 (ECCO Consortium 2017b) focusses on the flow fields and meteorological variables. Intended for later parts are discussions of the adjoint model (the dual model of Lagrange multipliers and sensitivities), and a formal analysis of the uncertainties. Fukumori et al. (2017) described the major changes from earlier ECCO estimates. Numerous discussions of various fields, beyond what we have space for here, such as bottom pressure, regional and global sea level, air-sea transfers, etc., means and variations, are listed in the references of these other papers.

In the spirit of a climatology, and in the interests of an easily workable volume of numbers, the discussion here is limited to the 20-year average, the 20-year average months (January, February,...), the 20-year average seasonal cycle (JJA, etc.), and the yearly averages 1994, 1995,...,etc.

Of necessity, only a few representative fields are shown here and with a few applications chosen to portray some of the more interesting or useful products. In an ocean state with 50-levels in the vertical, and strong geographical variability, each depth and region is at least slightly different from any other, and a complete depiction and rationalization is not possible within normal journal space limits. Additional fields and products can be seen in the online documents or in the many references given there. None of these results should be regarded as definitive; they are presented chiefly as an invitation to any interested scientist to recompute them as desired with different assumptions, averaging, etc.

The model native grid is shown in Figs. 2, 3 taken from Forget et al. (2015). Eddy fields are necessarily parameterized and not resolved. As Forget et al. (2015) discuss, at high northern latitudes

a distorted grid is used to avoid the polar singularity. Complexity of the high latitude gridding is one of the motivations for producing this easier-to-use climatology. An interpolation to a simple latitude/longitude grid has been used here for mapping purposes. Display of fields on the native grid, including high latitudes, can be seen in the various references and on the ECCO website. High latitudes have sometimes been omitted here where the presence of seasonal or permanent sea ice complicates the interpretation (e.g., salinity budgets). A specific high-northern-latitude version of the state estimate and its corresponding climatology is in preparation (A. Nguyen, personal communication 2017). Elsewhere longitudes are uniformly spaced at 1° and latitudes telescope toward the equator and pole. Over most of the oceanic domain, grid latitude distances maintain nearly constant grid areas.

a. Hydrography

Potential Temperature

An example of a twenty-year average hydrographic section is shown in Fig. 4 and which can be compared to the nearby quasi-synoptic WOCE section in Fig. 5. The gross structures are identical, but the average field is considerably smoother than is the WOCE section. Because much of the data used to produce the WOCE Atlases (http://woceatlas.ucsd.edu/; and see Schlitzer, 2017) were also used in the state estimate, large-scale gross structures in the ocean circulation can be seen readily in the various WOCE Atlases, and so are not reproduced here. Fig. 6 shows one example of a global thermal section at 14°N and Figs. 7, 8 are example temperatures at fixed depth levels. (Color coding here often follows that suggested by Thyng et al. (2017) to both accommodate color-blind readers and to avoid inadvertent emphasis of some features.) These and other fields are time averages consistent with the time mean flow and meteorological fields displayed below.

In many cases, a histogram of values is shown as an inset. Inevitable outliers (usually within topographically complex areas beyond the model resolution) are omitted in most plots.

Time-Dependence

Elements of the fluid ocean change constantly. As examples, Figs. 9, 10 show the estimated annual mean anomalies at 105m for two different years. Figure 11 is the 20-year average seasonal anomaly in December-January-February at 5m. All charts, despite the 20-year averaging, retain a spatial complexity that emphasizes the challenges of forming adequately accurate global averages. The annual anomalies (with spatial distributions not shown here) permit calculation of the changing heat content of the ocean over 20 years, shown as the corresponding temperature changes at different levels in Fig. 12. Error estimates are described briefly below, and are obtained from bootstrap estimates derived from the spatial distributions of temperature with systematic effects first having been suppressed. Upper levels are noisy while the deeper ones can be interpreted as showing simple linear trends. These and other products become part of the discussion of the oceanic heat uptake, the putative slowdown in atmospheric warming ("hiatuses"), etc. (see Wunsch and Heimbach 2014; Medhaug et al. 2017; Liang et al. 2017b).

Salinity

As a least-squares estimate, the ECCO state leaves explicitly computed misfits by month, year, and on the average. As an example, Fig. 13 shows the gridded 20-year mean misfit to the salinity data at 5m and 2084m. Apart from outliers in the Labrador Sea and other shallow regions (see e.g., Fenty and Heimbach 2013), the observations are generally within 0.5 on the practical salinity scale over most of the ocean. The implications of regional misfits for overall behavior of the state estimate would apply to any model calculation, whether constrained or not. In the present situation,

the Lagrange multipliers (adjoint or dual solution) are available for a sensitivity determination, but their use is not pursued here.

The time-average salinity field at one depth is shown in Fig. 14. The histogram insert shows a multi-modal distribution of values. Two 20-year average zonal sections of salinity are displayed in Figs. 15, 16 along the equator, and through the Drake Passage, respectively. A great deal of structure remains even after 20 years of averaging.

b. Pressure and Flow Fields

Surface Elevation

Surface elevation, $\eta(\theta,\lambda,t)$, relative to an estimated geoid is partially, but not completely, determined by the altimetric data: the state estimate is simultaneously being fit to meteorological forcing, the thermal, salinity and ice-cover fields, and any other data (e.g., gravity and altimeter height changes) that are present. A full determination of which elements of which observations are controlling the field depends upon the adjoint sensitivity of estimated η to each of these data sets. But because the altimetric records are the only ones nearly uniform and global over the entire 20 years, the 20-year average misfit to the time-varying altimetric measurement of η is shown in Fig. 17. Apart from outliers that have been suppressed in the charts, the misfits are generally within 10cms overall, highest at high latitudes, and showing some residual structures in the tropics. Misfits associated with the moving western boundary currents also appear. Explanations of residual misfits involves discussion of possible improvement by further iteration of the least-squares minimization, model errors including resolution issues and inadequate parameterization, and incomplete understanding of the observational errors. These will usually be functions of geographical position and possibly time, including seasonal effects.

Elevation and Pressure

The time-average dynamic topography, relative to the GRACE geoid, appears in Fig. 18 and again shows the classical gyres. Dynamic topography differs from η in the ice covered region where the pressure load is accounted for. Anomaly of η in 1997 appears in Fig. 19 and is the anomaly of dynamic topography in the ice-free regions.

Hydrostatic pressure fields, including bottom values, are also available; see e.g., Piecuch et al. (2015). Temporal variations are discussed by Forget and Ponte (2015) and Sonnewald et al. (2018).

Flow-Fields

The 20-year average horizontal components of Eulerian velocity (u, v) are displayed in Fig. 18 at 105m, and in Fig. 20 at 1000m These include both the geostrophic and ageostrophic components. The 1000m flows are readily compared e.g., to the results of Ollitrault and Colin de Verdière (2014) from Argo trajectories alone and which are noisier.

A zonal flow anomaly in 1995 in the Drake Passage is shown in Fig. 21. Annual average velocity anomalies are very small, but between 1994-2013 (not shown) produce a transport variability between -5 and +3Sv. Integration across a complex velocity structure is required to obtain the transports.

The Eulerian vertical velocity, w, is a crucial element in the oceanic general circulation, especially in the vorticity balance. Fig. 22 displays the 20-year mean w pattern at 105 m, a rough equivalent to the Ekman depth. Sign changes correspond to the classical gyre circulation as well as to the intense equatorial and coastal upwelling phenomena. At great depths (not shown), the pattern rapidly becomes complex beyond simple verbal description, and particularly as topographic features are approached from above (see Liang et al. 2017a for a discussion including that of the bolus velocity, w_b, and its sum with w.).

c. Meteorological Values

Meteorological forcing variables of wind, surface air temperature, specific humidity, precipitation, and radiative fluxes from the ERA-Interim reanalysis (Dee et al. 2011, 2014) are among the prior estimates of the control variables. As is well-known from a number of comparisons with other reanalysis products (e.g., Bromwich et al. 2007, 2015), none of these values can be regarded as very accurate. Chaudhuri et al. (2013, 2016) have discussed the errors that are assigned to them. In the process of determining the state estimate, these meteorological fields are adjusted so that the subsequent calculation with the free-running model, using the modified controls, renders it consistent with the ocean data. In general, the adjustments to the controls are small (see Fig. 23). A general result is a strengthening of the zonal winds both in the regions of high latitude westerlies and lower latitude easterlies. The adjustments in τ_x are skewed towards positive values, while the meridional ones (not shown) are more symmetric and weaker.

The estimated wind stress along with the surface flows permits calculation of the rate of working of the wind on the ocean circulation. Because, like the heat and freshwater transports, it depends upon second order products $\langle \mathbf{v} \cdot \boldsymbol{\tau} \rangle$, only the map of $\langle u \rangle \langle \tau_x \rangle$ is displayed as an example (Fig. 24) Results such as these are an important part of the ongoing attempts to understand the oceanic circulation energy budgets. Cf. Wunsch (1998), Zhai et al. (2012), Roquet et al. (2011).[2]

d. Mixed-Layer Depth

The oceanic mixed-layer depth is a function both of the meteorology and oceanic dynamics. Using the Kara et al. (2000, 2003) definition based on density changes, Fig. 25 displays the 20-year mean mixed-layer depth. As expected (not shown), considerable seasonal changes exist in these values.

[2] A full discussion of the rates of wind work requires strong assumptions about the averaging interval chosen for values, hourly, monthly, annual, etc. and is not pursued here.

3. Dynamics

A full discussion of oceanic circulation dynamics is far beyond the intended scope of this overview. As one example of possibilities, Fig. 26 displays a Rossby number, $Ro = UL/f$ at 722m, where a fixed value of $L = 100$km is used with the 20-year average horizontal speed. Apart from the equator, where it is not a useful measure of flow linearity, values of *Ro* are generally of order 0.001, consistent with linear dynamics. Other Rossby number definitions can be used (e.g., from the vorticity field) and many other non-dimensional parameters such as Ekman and Reynolds numbers can be computed.

A second example is shown in Fig. 27 as the 20-year average angle between the ageostrophic component of the surface flow and the 20-year average wind stress. With some exceptions, the estimated angle is not far from the canonical $\pm 45^\circ$, changing sign across the equator. In the southern hemisphere, the most probable angle is -55°, and in the northern hemisphere it is 66°. The ageostrophic flow was calculated as the the 5m total flow minus the geostrophic component from the mean dynamic topography in Fig. 18. A number of assumptions go into the production of the conventional 45°, including accuracy of the stress estimate, having the true surface velocity, and the nature of the turbulence within the Ekman-like layer.

Eddy physics, in the form of bolus velocities and vertical and horizontal mixing coefficients and viscosities can also be discussed using state-estimate products. These will be displayed and described more fully elsewhere.

4. Regional Studies

Regional oceanographic subsets are easily extracted from the global files as annual, seasonal etc., averages. A very large number of interesting regional studies is possible, bearing in mind the resolution problems near boundaries. As an example of what can be done regionally with

salinity, Fig. 28 displays the twenty-year seasonal average anomalies at 5m depth of salinity in the Bay of Bengal (see e.g.,the special issue *Oceanography*, 29(2) 2016) for a comparison). Regional applications of the climatology can be seen in Wunsch and Heimbach (2013b), Buckley et al. (2014, 2015), Evans et al. (2017), and Piecuch et al. (2017), all with a focus on the Atlantic Ocean.

5. Uncertainties

Determining uncertainties in results of "pure" data climatologies, data-constrained state estimates such as this one, and in conventional unconstrained coupled or uncoupled models are a difficult problem for many reasons. These reasons range from model errors, inadequate resolution, and to a variety of problems connected with the observations. Boyer et al. (2016) discuss an upper- ocean 700m climatology and separated the errors into those due to mapping methods and to bias correction uncertainty, with methodology uncertainty dominating. A partial discussion of the uncertainties in the ECCO v4 estimate can be found in Wunsch (2017), where the stochastic error is separated, at least in part, from the systematic error. Thus, for example, the 20-year global temperature is found to be $3.5127^\circ \pm 0.0014^\circ (2\ \sigma)$ uncertainty and an approximate 20-year mean heating rate of 0.48 ± 0.004 W/m^2 with uncertainties being the formal error derived from a bootstrap method (Wunsch, 2017). Paradoxically, it is only the short interval of 20 years relative to the far longer times required for the ocean to adjust on a large scale that justifies the assumptions leading to the error estimates. We also emphasize, once again, that quantities such as ocean temperatures and their changes (as in Fig. 12) reflect the implications of *all* the data, including those derived from meteorology, altimetry, etc. and not just the direct thermal measurements, as well as the information content lying with the space-time evolution of the dynamical model.

6. Final Remarks

In brief, this 20-year ocean climatology differs from those more conventionally available in a number of ways:

(A) A large variety of near-global data sets combine to determine the state values. Each data type has specific error estimates and all quantities calculated reflect the influence of all data types. (B) Data, beginning in 1992, although not entirely homogeneous over the 20-year span, are nearly symmetric in distribution about the equator. (C) The values encompass the full water column and the entire ocean including the Arctic regions. (D) All conventional output values of a general circulation model, including three components of velocity, pressure, temperature, salinity, sea ice, and their computable products (e.g., heat content change or the vorticity budget) are available, along with meteorological estimates dynamically consistent with the oceanic fields. (E) All basic conservation rules for the ocean circulation including enthalpy, energy, etc., are obeyed to machine precision in the model equations.

Undoubtedly, a much longer averaging interval would produce quantitatively different results. A better (more accurate) estimate of the 20-year period 1994-2013 is also surely possible, but the existing state estimate is arguably the best now available, and it permits a useful discussion of oceanic changes and their governing physics over two decades.

The gist of this paper is that understanding the ocean either as an instantaneous picture, or as an average over any finite period, must confront the intense time-variability. Significantly improving the accuracy of future estimates, if interpreted as climatological averages, will not be easy, involving as it does the need for far longer records, much better observational coverage of the ocean below 2000m, and in specific regions, improved time-space resolution both of the observations

and of the underlying general circulation model. Better quantification of the error structures of all existing and future data sets is also very important.

7. Obtaining the State Estimate Values

A concise documentation of ECCO Version 4 Release 3 is given by Fukumori et al. (2017, 2018). The full state estimate values on the model native grid at monthly intervals 1992-2015 are available at ftp://ecco.jpl.nasa.gov/Version4/Release3/ in netCDF form and which includes the full suite of data used in the least-squares fitting. A subset of values making up the present climatology described here, 1994-2013, as described in ECCO Consortium (2017a,b) in MATLAB.mat files, can be found at http://mit.ecco-group.org/opendap/diana/h8_i48/. Additional documentation is available that describes how to analyze property budgets using these estimates (Piecuch 2017) and how to run the model to produce additional fields not available in the archive (Wang 2017). Any of the authors can be contacted for help and advice. Comments about difficulties or errors are welcomed.

Acknowledgments. ECCO has been funded over many years primarily by the National Aeronautics and Space Administration at MIT, AER, JPL at UT Austin. Supported in part through NASA Contract NNN12AA01C at JPL, and NASA GRACE grant NNH16CT00C at AER. Particular thanks are owed the NASA Program Manager, Eric Lindstrom, for his sustained support and advice.

References

AchutaRao, K. M., and Coauthors, 2007: Simulated and observed variability in ocean temperature and heat content. Proc. Nat. Acad. Scis., USA, 104, 10768-10773.

Adcroft, A., C. Hill, J. M. Campin, J. Marshall, and P. Heimbach, 2004: Overview of the formulation and numerics of the MIT GCM, ECMWF Proceedings, Shinfield Park, Reading UK, 139-150 pp., http://gfdl.noaa.gov/˜aja/papers/ECMWF–2004-Adcroft.pdf.

Boyer, T., and Coauthors, 2016: Sensitivity of global upper-ocean heat content estimates to mapping methods, XBT bias corrections, and baseline climatologies. J. Clim. , 29, 4817-4842.

Bromwich, D. H., Fogt, R. L., Hodges, K. I., Walsh, J. E., 2007: A tropospheric assessment of the ERA-40, NCEP, and JRA-25 global reanalyses in the polar regions. J. Geophys. Res.-Atm., 112.

Bromwich, D. H., Wilson, A. B., Bai, L.-S., Moore, G. W. K., Bauer, P., 2015: A comparison of the regional Arctic System Reanalysis and the global ERA-Interim Reanalysis for the Arctic. Quat. J. Roy. Met. Soc., 142(695), 644–658. http://doi.org/10.1002/qj.2527

Buckley, M. W., Ponte, R. M., Forget, G., Heimbach, P. (2014). Low-frequency SST and upper-ocean heat content variability in the North Atlantic. Journal of Climate, 27, 49965018.

Buckley, M. W., Ponte, R. M., Forget, G., Heimbach, P., 2015: Determining the Origins of Advective Heat Transport Convergence Variability in the North Atlantic. Journal of Climate, 28, 39433956.

Chaudhuri, A. H., R. M. Ponte, and G. Forget, 2016: Impact of uncertainties in atmospheric boundary conditions on ocean model solutions. Ocean Mod., 100, 96-108.

Chaudhuri, A. H., R. M. Ponte, G. Forget, and P. Heimbach, 2013: A comparison of atmospheric reanalysis surface products over the ocean and implications for uncertainties in air-sea boundary forcing. J. Clim. , 26, 153-170.

ECCO Consortium, 2017a: A Twenty-Year Dynamical Oceanic Climatology: 1994-2013. Part 1: Active Scalar Fields: Temperature, Salinity, Dynamic Topography, Mixed-Layer Depth, Bottom Pressure. (MIT DSpace), http://hdl.handle.net/1721.1/107613

———, 2017b: A Twenty-Year Dynamical Oceanic Climatology: 1994-2013. Part 2: Velocities and Property Transports. (MIT DSpace), http://hdl.handle.net/1721.1/109847.

Dee, D. P., M. Balmaseda, G. Balsamo, R. Engelen, A. J. Simmons, and J. N. Thépaut, 2014: Toward a consistent reanalysis of the climate System. Bull. Am. Met. Soc., 95, 1235-1248.

Dee, D. P., and Coauthors, 2011: The ERA-Interim reanalysis: configuration and performance of the data assimilation system. Quat. J. Roy. Met. Soc., 137, 553-597.

Evans, D. G., Toole, J., Forget, G., Zika, J. D., Naveira Garabato, A. C., Nurser, A. J. G., Yu, L., 2017: Recent wind-driven variability in Atlantic water mass distribution and meridional overturning circulation. Journal of Physical Oceanography, 47(3), 633647.

Fenty, I., and P. Heimbach, 2013: Coupled sea-ice-ocean-state estimation in the Labrador Sea and Baffin Bay. J. Phys. Oc., 43, 884-904.

Forget, G., D. Ferreira, and X. Liang, 2015: On the observability of turbulent transport rates by Argo: supporting evidence from an inversion experiment. Ocean Sci, 11, 839-853.

Forget, G., Ponte, R. M.: 2015: The partition of regional sea level variability. Progress in Oceanography, 137, 173195.

Forget, G., J.-M. Campin, P. Heimbach, C. Hill, R. Ponte, and C. Wunsch, 2015: ECCO version 4: an integrated framework for non-linear inverse modeling and global ocean state estimation. Geosci. Model Dev., 8, 3071-3104.

389 Fu, L.-L., and E. A. Cazenave, 2001: Satellite Altimetry and Earth Sciences. A Handbook of
390 Techniques and Applications. Academic, San Diego, 463 pp.

391 Fukumori, I., O. Wang, I. Fenty, G. Forget, P. Heimbach, and R. Ponte, 2017: ECCO Version 4
392 Release 3. ftp://ecco.jpl.nasa.gov/Version4/Release3/doc/v4r3_summary.pdf.

Fukumori, I., I. Fenty, G. Forget, P. Heimbach, C. King, A. Nguyen, C. Piecuch, R. Ponte, K. Quinn, N. Vinogradova, and O. Wang, 2018: Data sets used in ECCO Version 4 Release 3. ftp://ecco.jpl.nasa.gov/Version4/Release3/doc/v4r3$_data.pdf$.

393 Ganachaud, A., Wunsch, C., 2000:. Improved estimates of global ocean circulation, heat
394 transport and mixing from hydrographic data. Nature, 408(6811), 453-457. http://doi.org/-
395 10.1038/35044048.

396 Gebbie, G. and P. Huybers, 2017: The little ice age and 20th-Century deep Pacific cooling.
397 Submitted for publication.

398 Gent, P. R., and J. C. Mcwilliams, 1990: Isopycnal mixing in ocean circulation models. J. Phys.
399 Oc., 20, 150-155.

400 Gouretski, V. V.,. Koltermann, K. P., 2004: WOCE Global Hydrographic Climatology., Berichte
401 des Bundesamtes für Seeschifffahrt und Hydrographie Nr. 35/2004, Hamburg and Rostock, 50 pp.

402 Ishii, M., Kimoto, M., Kachi, M., 2003:. Historical ocean subsurface temperature analysis with
403 error estimates. Mon. Weath. Rev., 131(1), 51–73. http://doi.org/10.1175/1520-0493(2003)131.

404 Kara, A. B., P. A. Rochford, and H. E. Hurlburt, 2000: An optimal definition for ocean
405 mixed layer depth, J. Geophys. Res., 105(C7), 16803–16821, doi:10.1029/2000JC900072
406 http://doi.org/10.1002/qj.2527

407 Kara, A. B., P. A. Rochford, and H. E. Hurlburt, 2003: Mixed layer depth variability over the
408 global ocean. J. Geophys. Res., 108, 3079.

Kennedy, J. J., N. A. Rayner, Smith, R. O., D. E. Parker, and M. Saunby, 2011: Reassessing biases and other uncertainties in sea surface temperature observations measured in situ since 1850: 2. Biases and homogenization. J. Geophys. Res., 116.

Knudsen, P., and R. Bingham, Andersen, O., Rio, M. H., 2011: A global mean dynamic topography and ocean circulation estimation using a preliminary GOCE gravity model. J. Geod., 85, 861-879.

Koltermann, K. P., V. V. Gouretski, and K. Jancke, Eds., 2011: Hydrographic Atlas of the World Ocean Circulation Experiment (WOCE). Volume 3: Atlantic Ocean International WOCE Project Office, Southampton, UK, ISBN 090417557X.

Levitus, S., 1982: Climatological Atlas of the World Ocean, 173 pp plus microfiche NOAA Professional Paper 13.

Liang, X., C. Wunsch, P. Heimbach, and G. Forget, 2015: Vertical redistribution of oceanic heat content. J. Clim., 28, 3821-3833, 2550-2562

Liang, X., M. Spall, C. Wunsch, 2017a: Global ocean vertical velocity from a dynamically consistent ocean state estimate, J. Geophys. Res., 122 , 8208-8224

Liang, X., C. G. Piecuch, R. M. Ponte, G. Forget, C. Wunsch, P. Heimbach, 2017b: Change of the global ocean vertical heat transport over 1993-2010, J. Clim., 30, 5319-5327.

Lumpkin, R. and K. Speer, 2007: Global ocean meridional overturning, J. Phys. Oc., 37,, 2550-2562.

Marshall, J., A. Adcroft, C. Hill, L. Perelman, and C. Heisey, 1997: A finite-volume, incompressible Navier Stokes model for studies of the ocean on parallel computers. J. Geophys. Res.-Oceans, 102, 5753-5766.

Maximenko, N., and Coauthors, 2009: Mean dynamic topography of the ocean derived from satellite and drifting buoy data using three different techniques. J. Atm. Oc. Tech., 26, 1910-1919.

433 Medhaug, I., Stolpe, M. B., Fischer, E. M., Knutti, R., 2017:. Reconciling controversies about
434 the “global warming hiatus.” Nature, 545(7652), 41–47. http://doi.org/10.1038/nature22315
435 Ollitrault, M. and A. Colin de Vèrdiere, 2014: The ocean general circulation near 1000-m depth.
436 J. Phys. Oc., 44, 384-409.
437 Piecuch, C. G., 2017:, A note on evaluating budgets in ECCO Version 4 Release 3. ftp:-
438 //ecco.jpl.nasa.gov/Version4/Release3/doc/evaluating_budgets_in_eccov4r3.pdf.
439 Piecuch, C. G., I. Fukumori, R. M. Ponte, O. Wang, 2015: Vertical structure of ocean pressure
440 variations with application to satellite-gravimetric observations. J. Atm. Oc. Tech., 32, 603-613.
441 Piecuch, C. G., Heimbach, P., Ponte, R. M., Forget, G. L.: 2015: Sensitivity of contemporary
442 sea level trends in a global ocean state estimate to effects of geothermal fluxes. Ocean Modelling,
443 96, 214220.
444 Quinn, K. J., and R. M. Ponte, 2008: Estimating weights for the use of time-dependent grav-
445 ity recovery and climate experiment data in constraining ocean models, J. Geophys. Res., 113,
446 C12013, doi:10.1029/2008JC004903.
447 Roemmich, D., and Coauthors, 2009: The Argo Program: Observing the global ocean with
448 profiling floats. Oceanog., 22, 34-43.
449 Reynolds, R. W. and Smith, T. M., 1994. Improved global sea surface temperature analyses
450 using optimum interpolation. J. Clim., 7, 929-948.
451 Reynolds R. W. and Smith, T. M., 1995: A high resolution global sea-surface climatology. J.
452 Clim., 8, 1571-1583.
453 Riser, S. C., Freeland, H. J., Roemmich, D., Wijffels, S., Troisi, A., Belbéoch, M., et al., 2016:.
454 Fifteen years of ocean observations with the global Argo array. Nature Clim. Change, 6(2), 145–
455 153. http://doi.org/10.1038/nclimate2872

Roquet, F., Wunsch, C., Madec, G., 2011: On the patterns of wind-power input to the ocean circulation. J. Phys. Oc., 41, 2328-2342.

Roquet, F., and Coauthors, 2013: Estimates of the Southern Ocean general circulation improved by animal-borne instruments. Geophys. Res. Letts., 40, 6176-6180.

Schlitzer, R., 2017: Ocean Data View, odv.awi.de,.

Siedler, G., S. Griffies, Gould, J., Church, J. , Eds., 2013: Ocean Circulation and Climate, 2nd Ed. A 21st century perspective. Academic Press.

Sonnewald, M., C. Wunsch, P. Heimbach, 2018: Linear predictability: A sea surface height case study. J. Climate, in press.

Stammer, D., C. Wunsch, R. Giering, C. Eckert, P. Heimbach, J. Marotzke, A. Adcroft, C. Hill, J. Marshall, 2003: Volume, heat and freshwater transports of the global ocean circulation 1992-1997, estimated from a general circulation model constrained by WOCE data. J. Geophys. Res., 107, C9.

Stammer, D., and Coauthors, 2002: Global ocean circulation during 1992-1997, estimated from ocean observations and a general circulation model. J. Geophys. Res.-Oceans, 107, C9

Stammer, D., Balmaseda, M., Heimbach, P., Köhl, A., Weaver, A., 2016:. Ocean data assimilation in support of climate applications: Status and perspectives. Ann. Rev. Mar. Sci., 8, 491–518. http://doi.org/10.1146/annurev-marine-122414-034113

Talley, L. D., and Coauthors, 2016: Changes in ocean heat, carbon content, and ventilation: A review of the first decade of GO-SHIP Global Repeat Hydrography. Ann. Rev. Mar. Sci., Vol 8, 185-215.

Thyng, K. M., C. A. Greene, R. D. Hetland, H. M. Zimmerle, and S. F. DiMarco, 2016: True colors of oceanography. Guidelines for effective and accurate colormap selection. Oceanog., 29, 9-13.

Wang, O., 2017: Instructions for reproducing ECCO Version 4 Release 3. ftp://ecco.jpl.nasa.gov/Version4/Release3/doc/ECCOv4r3_reproduction.pdf.

Watkins, M. M., Wiese, D. N., Yuan, D.-N., Boening, C., Landerer, F. W., 2015: Improved methods for observing Earth's time variable mass distribution with GRACE using spherical cap mascons. J. Geophys. Res.: Solid Earth, 120(4), 2648–2671. http://doi.org/10.1002/2014JB011547

Wunsch, C., 1998: The work done by the wind on the oceanic general circulation. J. Phys. Oc., 28, 2332-2340.

Wunsch, C., 2016: Global ocean integrals and means, with trend implications. Ann. Rev. Mar. Sci., Vol 8, C. A. Carlson, and S. J. Giovannoni, Eds., 1-33.

Wunsch, C., 2017: Uncertainties in Mean and Changes in Heat, Salt, and Surface Elevation in the Global Ocean Submitted for publication.

Wunsch, C., and P. Heimbach, 2007: Practical global oceanic state estimation. Physica D-Nonlin. Phen., 230, 197-208.

——, 2013: Dynamically and kinematically consistent global ocean circulation state estimates with land and sea ice. Ocean Circulation and Climate, 2nd Edition, J. C. G. Siedler, W. J. Gould, S. M. Griffies, Eds., Ed., Elsevier, 553-579.

——,2014: Bidecadal thermal changes in the abyssal ocean and the observational challenge. J. Phys. Oc., 44 2013-2030.

Wunsch, C., P. Heimbach, R. M. Ponte, I. Fukumori, and ECCO Consortium Members, 2009: The global general circulation of the ocean estimated by the ECCO-Consortium. Oceanog., 22, 88-103.

Zhai, X. M., and H. L. Johnson, Marshall, D. P., Wunsch, C., 2012: On the wind power input to the ocean general circulation. J. Phys. Oc., 42, 1357-1365.

LIST OF FIGURES

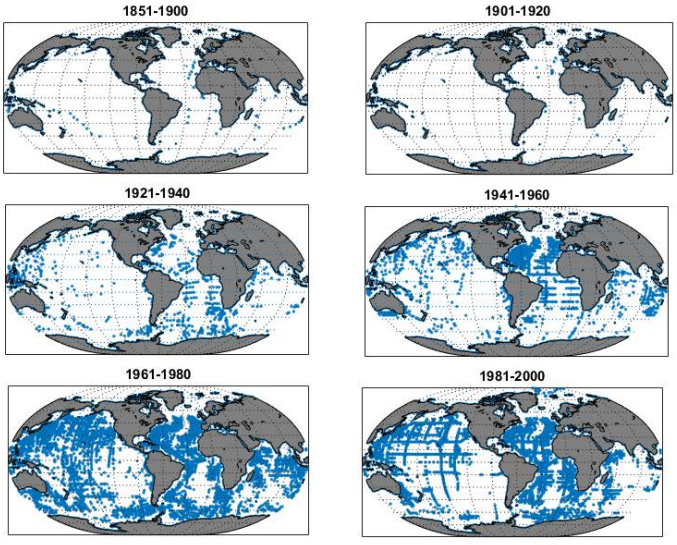

FIG. 1. Hydrographic measurements reaching at least 3600m between (a) 1851 and 1900, and then in 20-year increments to 2000. From WOA. See Wunsch (2016) for corresponding data distributions to 2000m. Early years have a North Atlantic bias, and all years have seasonal biases (not shown) towards low latitudes in winter. Although crude spatial averages could have been formed as early as 1900, even in later decades their accuracy would have been poor. In some cases, shallow topographic features such as the mid-ocean ridges are apparent as blank spaces (e.g., the North Atlantic 1941-1960).

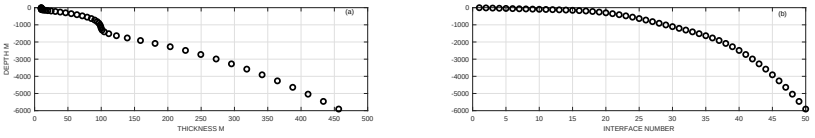

FIG. 2. (a) Layer thicknesses; (b) level depths in the ECCO version 4 state estimate, both in meters. (See Forget et al., 2015).

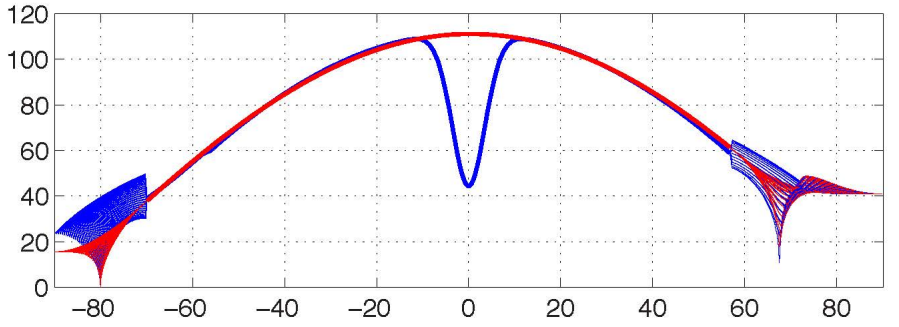

FIG. 3. Latitude (blue curve) and longitude spacing in kilometers as a function of latitude (from Forget et al., 2015). Closer latitude spacing exists near the equator. At high latitudes the complex grid leads to a distribution of spacings (see Figs. 1,2 of Forget et al., 2015). Most of the high latitude southern region is land. At mid-latitudes, horizontal cell areas are nearly constant. For the mapping, the meridional grid spacing is preserved except in the high latitude regions, where it is replaced by a uniform 1 degree interpolation grid.

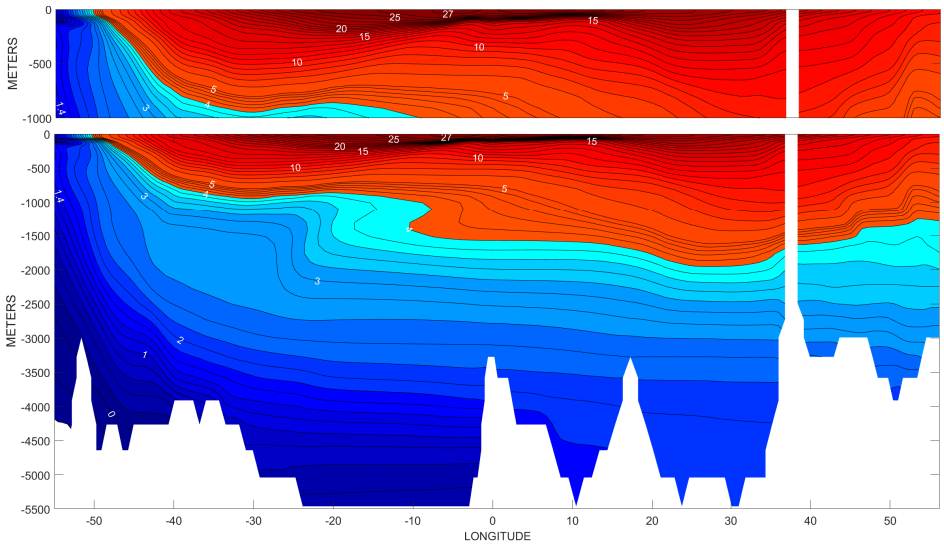

FIG. 4. Twenty-year mean section of potential temperature (°C) down 25°W in the Atlantic ocean. Region in white is bathymetry. The section is smoother than any quasi-synoptic section would be, although considerable structure remains despite the averaging time. Compare to Fig. 5 showing quasi-synoptic shipboard measurements from the late 1980s. Color coding is similar but not identical.

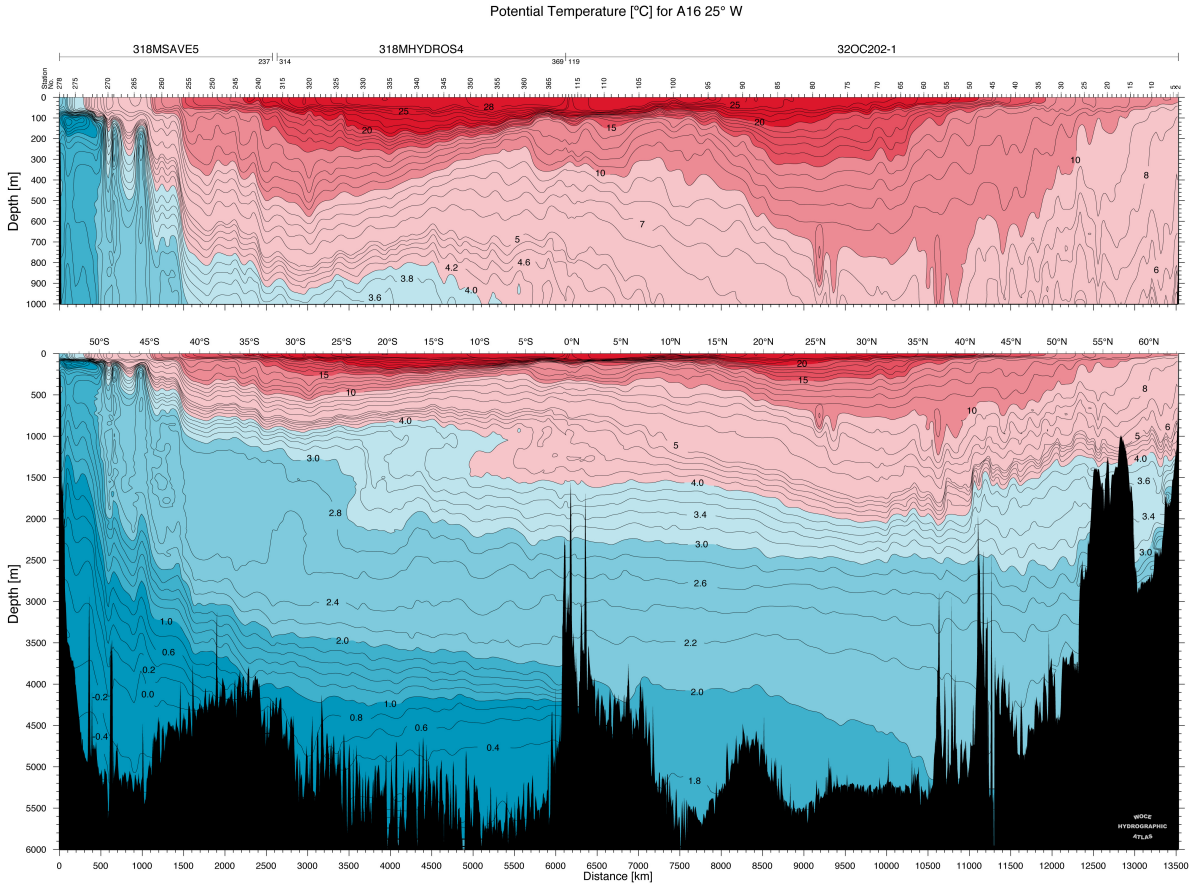

FIG. 5. WOCE section of potential temperature (°C) nominally down 25°W in the Atlantic Ocean, although the ships deviated from that longitude. From Koltermann et al. (2011). Notice the presence of much small scale structure of several degrees of latitude not present in the 20-year mean section (Fig. 4). Note that data used to produce the published Atlas plate were obtained in 1988 and 1989, while additional WOCE data on this line, used in the state estimate, were measured during the specific climatology interval. Differences from those observations are a part of the data misfit discussion and are dominated by the small scales (not shown).

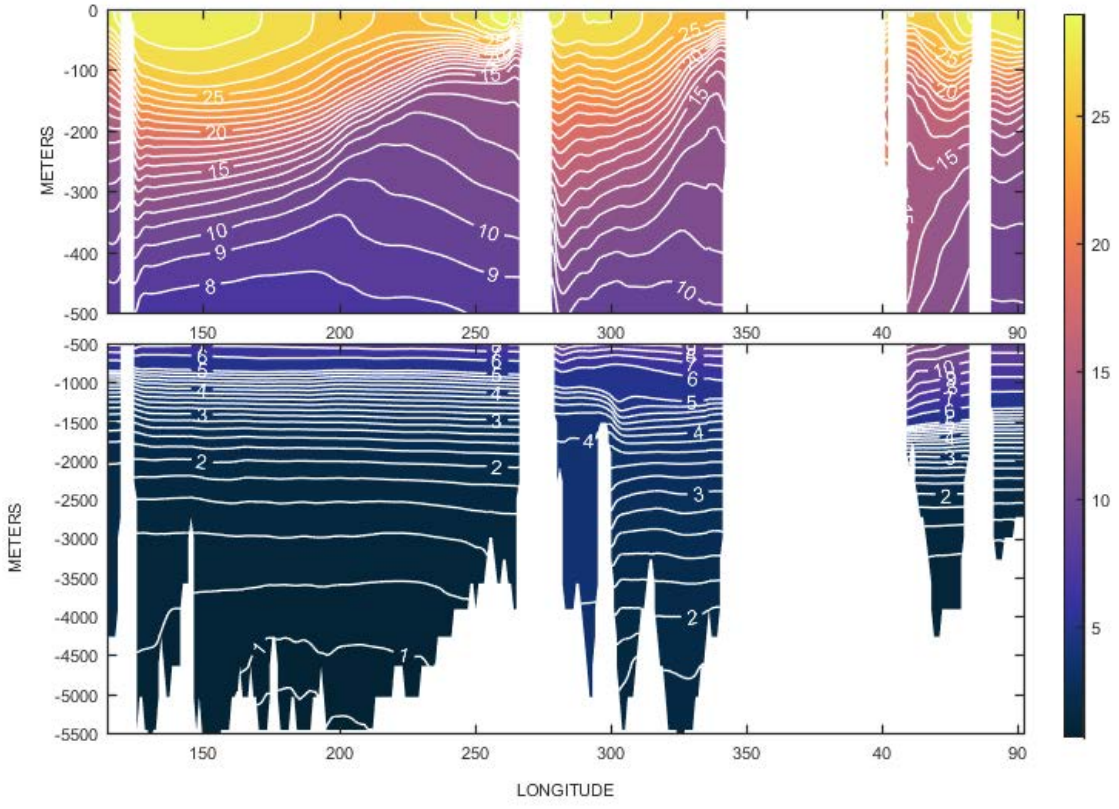

FIG. 6. Twenty-year mean potential temperature (°C) in all three oceans along 14°N. Both Atlantic and Pacific Oceans display the expected eastward tilt of the thermocline and with nearly flat isotherms at depth except where major topographic features are encountered.

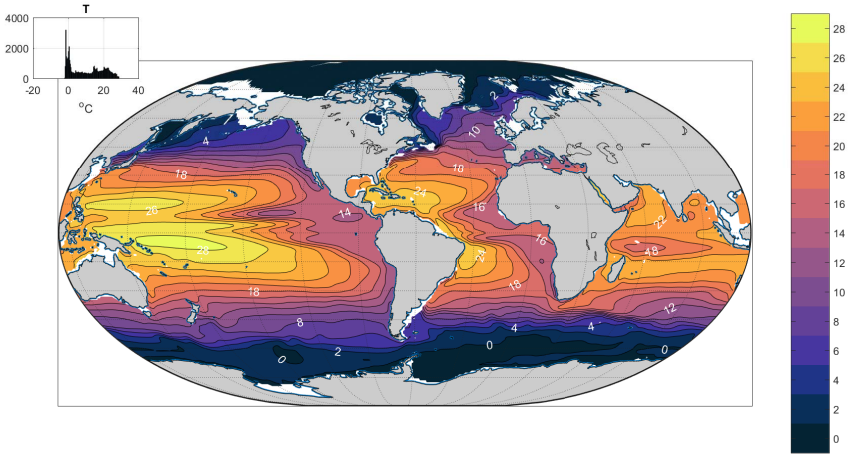

649 FIG. 7. Twenty-year average potential temperature at 105m (°C). Inset shows the histogram of values at
650 this depth. Dominant features are the subtropical gyres in all oceans and the relatively very cold water in the
651 Southern Ocean.

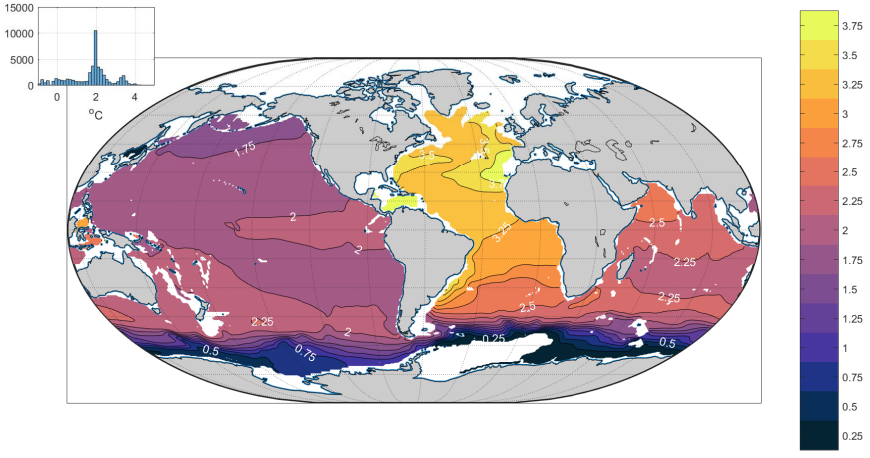

652 FIG. 8. Twenty-year average temperature at 2084m (°C). Color saturates at 3.9 °C with outlier maxima occur-
653 ring in the Mediterranean and Gulf of Mexico where the deep water resolution is inadequate for the topography.
654 The relative warmth of the North Atlantic Ocean is prominent.

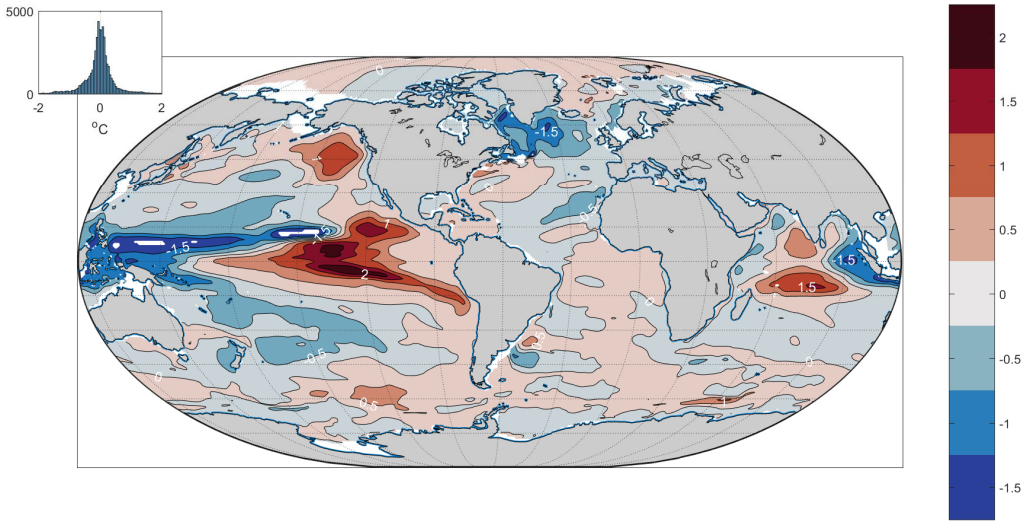

FIG. 9. Anomaly of temperature (°C) in 1994 relative to the 20 year mean at 105m. The complex spatial structure emphasizes the need for approximately uniformly distributed global measurements if accurate basin or global averages are sought.

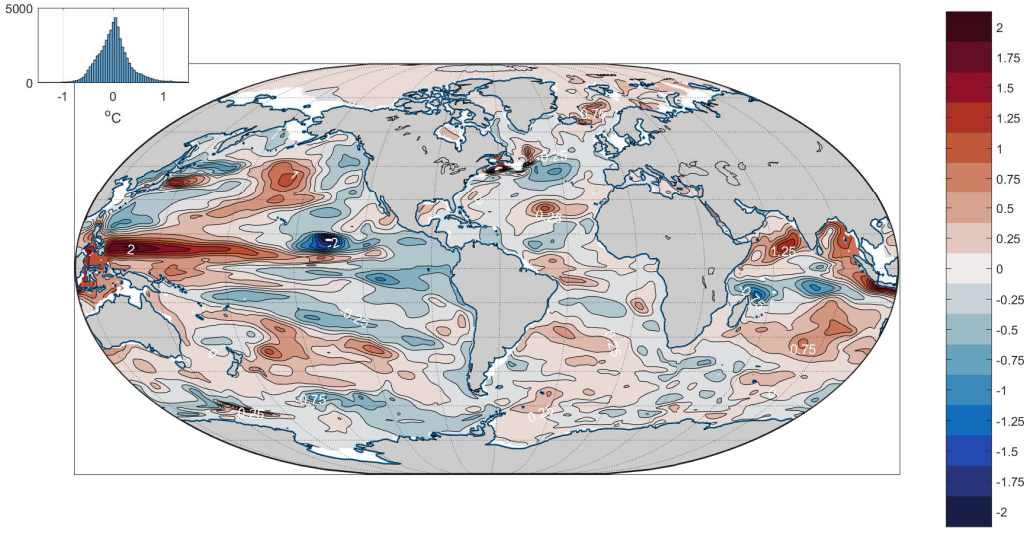

FIG. 10. Annual mean anomaly of temperature (°C) at 105m in 2013, twenty-years after that in Fig. 9.

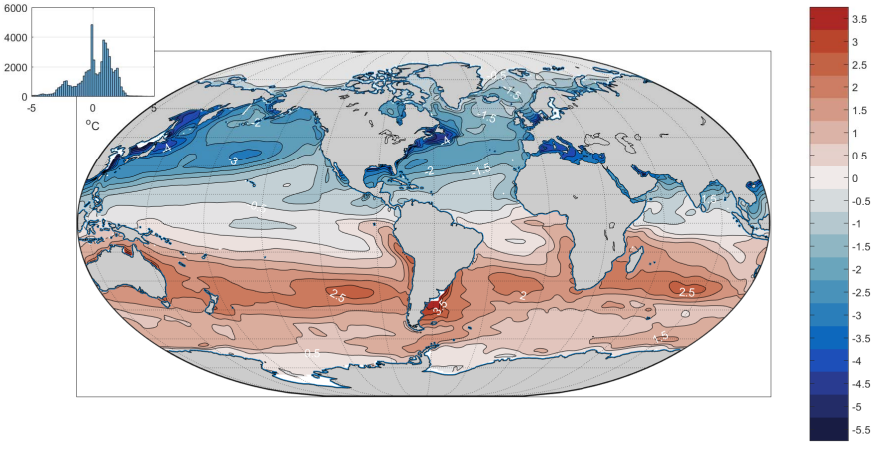

FIG. 11. Example of a 20-year average seasonal (December, January, February, DJF) mean 5m temperature (°C) anomalies relative to the 20-year mean. The main feature is the interhemispheric anti-symmetry with the conventional larger amplitudes in the northern region. Southern hemisphere boundary currents are conspicuous.

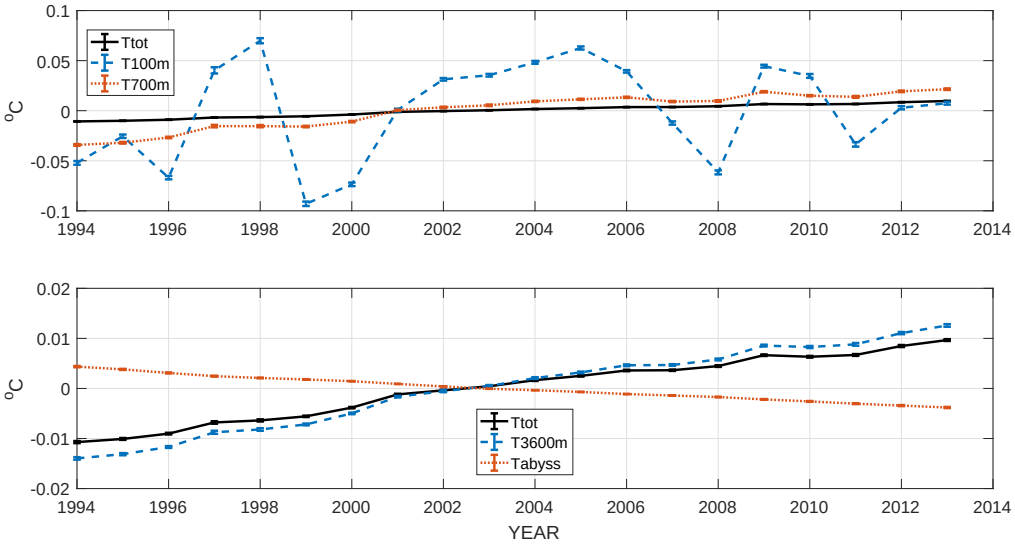

FIG. 12. Volume weighted temperature change (°C) by year. Upper panel is the average to 100m, 700m, and the total, top-to-bottom. Lower panel shows the averages to 3600m, the repeated total top-to-bottom, and the abyssal layer below 3600m which shows net cooling. Formal (stochastic component) error bars are for the annual volume mean as computed from a bootstrap method as described by Wunsch (2017). The deep cooling is discussed by Wunsch and Heimbach (2014) and rationalized by Gebbie and Huybers (2017).

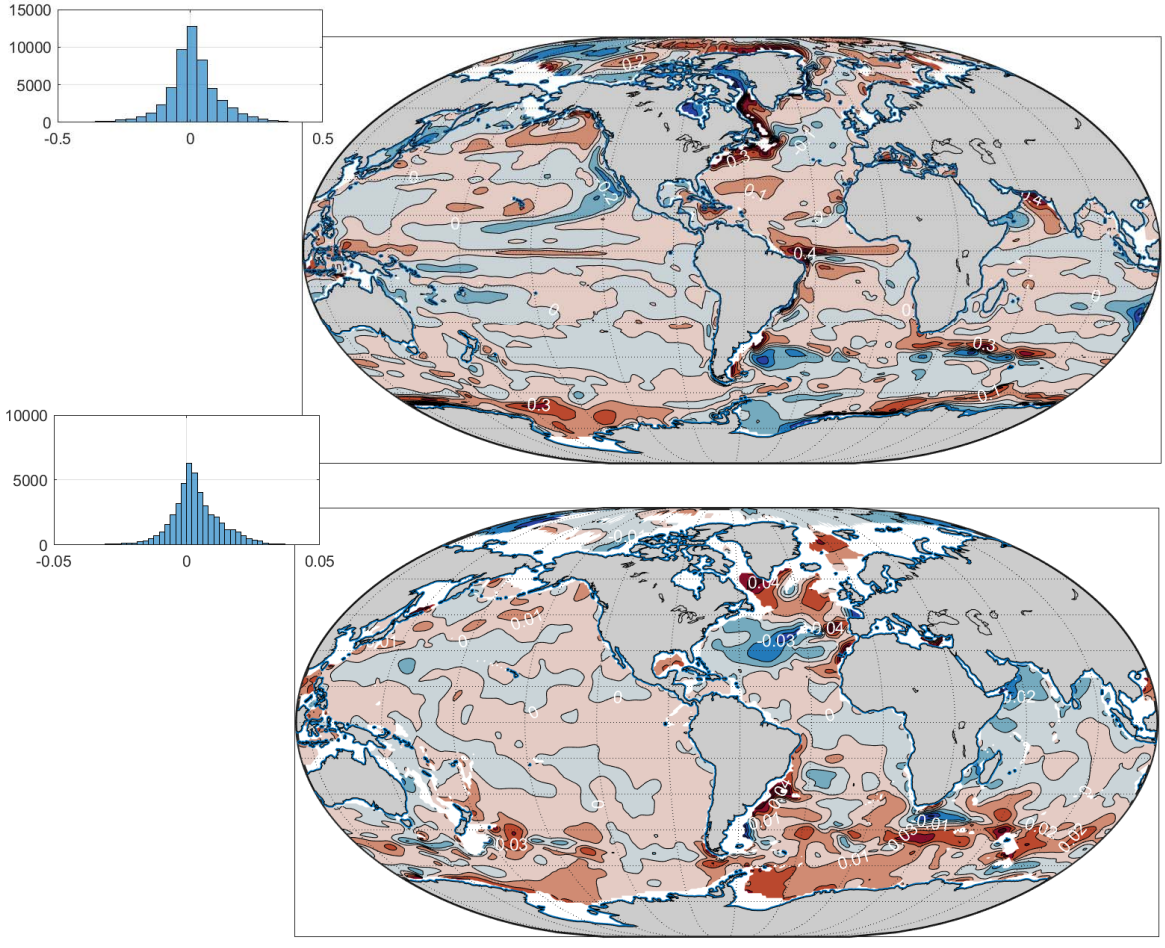

FIG. 13. (Upper panel) Misfit of the state estimate to the Gouretski and Kolermann (2004) salinity climatology (practical salinity scale)) averaged over 20 years at 105m. Histogram inset shows the distribution of values which is unimodal about 0 and close to Gaussian. Some isolated outliers are omitted. Major deviations are associated primarily with marginally resolved coastal and other jet-like currents, such as the Agulhas retroflected flow. (Lower panel). Same as upper panel except at 2084 m. Although not formally tested, the residuals have a visual resemblance to a stochastic field with regional variations; see the discussion in Wunsch (2017). Available fields permit computation of misfits to all observations used in the state estimate over months, years, seasons, and the duration and poisition including, where appropriate, as functions of depth.

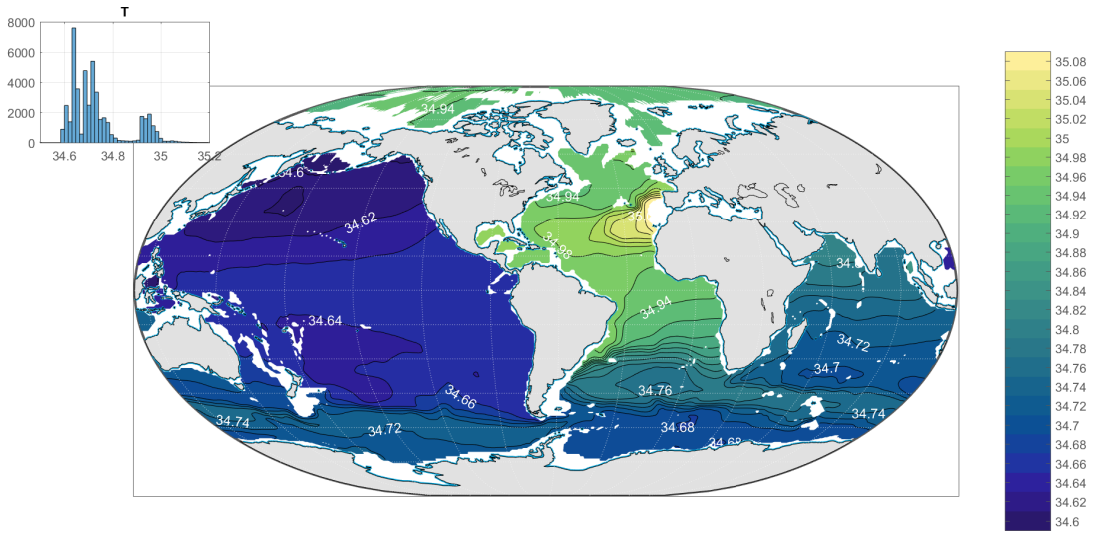

FIG. 14. Twenty-year average salinity (practical salinity scale) at 2084m. Excess values in the North Atlantic and the extreme of the Mediterranean Sea outflow (Mediterranean Sea values are truncated here) are visible. The relatively saline Atlantic Ocean is apparent, mimicking the thermal differences seen in Fig. 8.

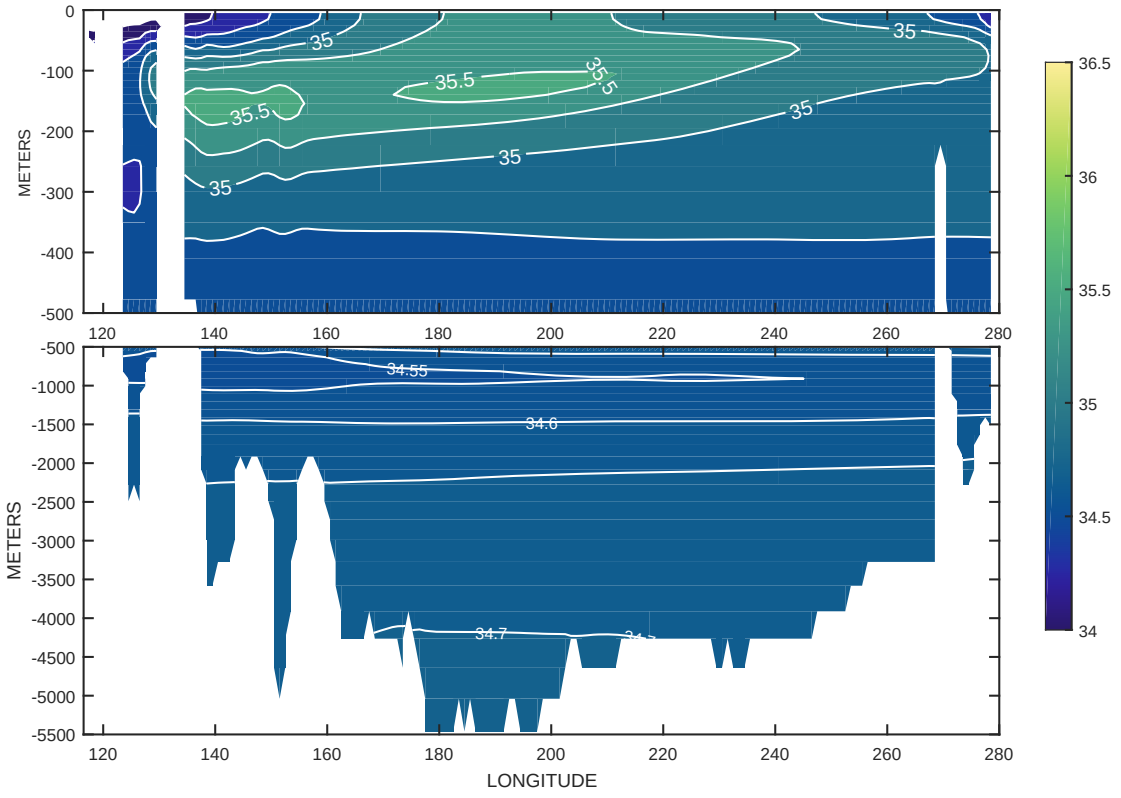

FIG. 15. Twenty-year average salinity (practical scale), in a zonal section along the equator in the Pacific Ocean. Note extra contours below 500m. Steep upward slope of the halocline to the east is part of the discussion of time-mean equatorial dynamics.

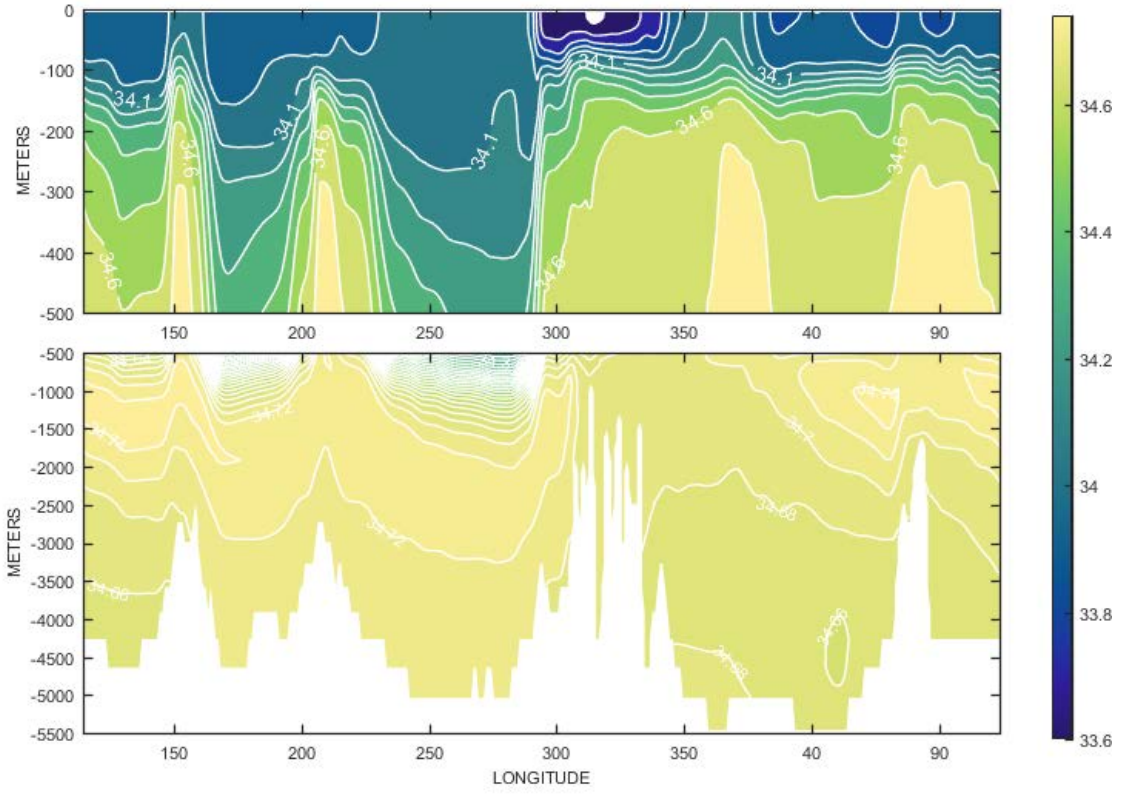

FIG. 16. Twenty-year mean salinity (practical scale) in a zonal section through the Drake Passage (60°S) with a complex zonal structure as seen also in temperature (not shown here; see ECCO Consortium 2017a) and producing a similarly complex zonally varying $T - S$ relationship in the Southern Ocean.

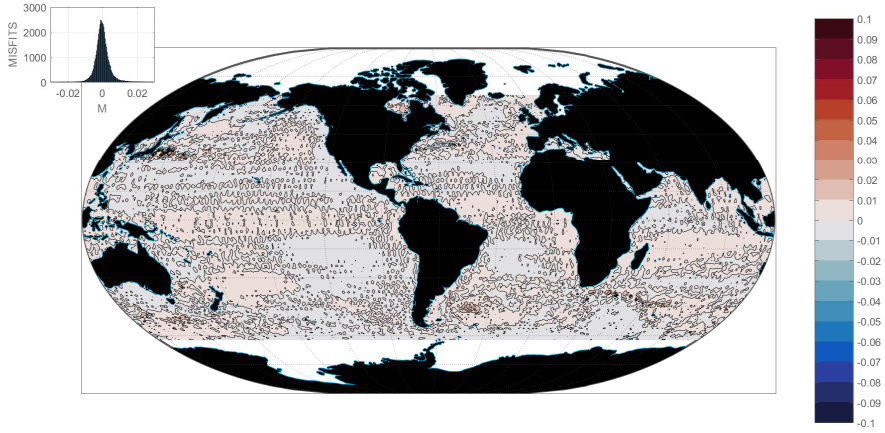

FIG. 17. Average misfit (m) over 20 years of the state estimated values of η and that measured by the suite of TOPEX/POSEIDON-Jason altimeters. Based upon the average of the monthly misfits in the generally ice-free region. Weighting operators were chosen so that small scale features are ignored in the least-squares fitting, as they are dominated by geoid error and mesoscale features. Unimodality-about-zero character of the residuals is clear, but large-scale patterns suggest residual systematic errors in the altimeter data or in the model of order 2cm. Complex detail of the zero contour, which dominates the plot, is consistent with a zero-mean, nearly random, residual. As with the salinity misfit in Fig. 13 these fields are computable over arbitrary data intervals within the 20-year climatology time-span.

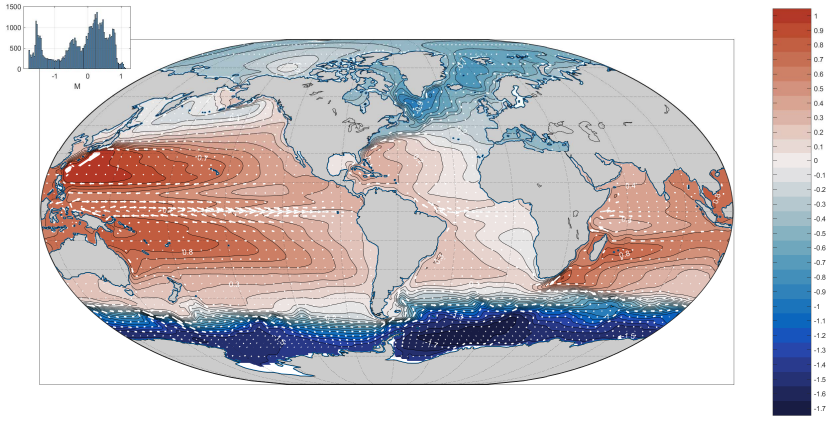

FIG. 18. Twenty-year mean dynamic topography (m) from the model mean sea surface elevation. Values in ice-covered regions are corrected for the ice load and differ there for equivalent sea level. Off-setting the entire surface by a constant would have no observable dynamical consequences. Compare to Maximenko et al. (2009), Knudsen et al. (2011). Inset shows the histogram of values about the mean. The overall range is about 3m. Arrows show the flow field, which dominantly geostrophic, at 105m depth.

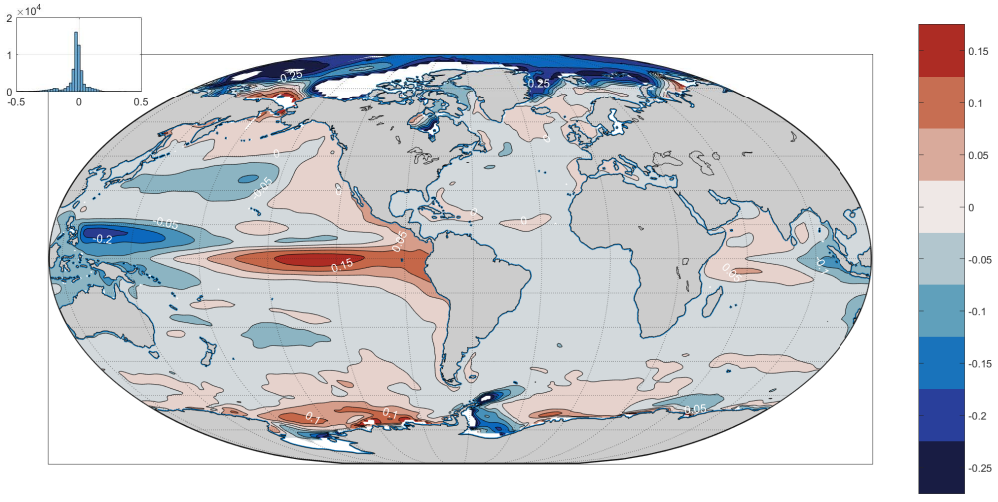

FIG. 19. Average of the anomaly of surface elevation η (m) during El Niño year (1997) with the expected elevation excess in the eastern Pacific Ocean. Structure elsewhere becomes part of the discussion of the global elements of ENSO.

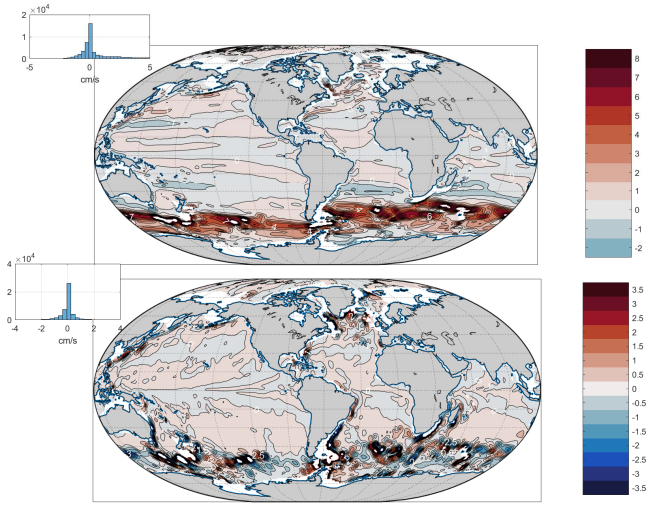

FIG. 20. Twenty-year average horizontal flow (cm/s) at 1000m. Upper panel is the zonal component, u and lower panel is the meridional component v. Note the different color scales. Compare to Ollitrault and Colin de Verdière, 2014.

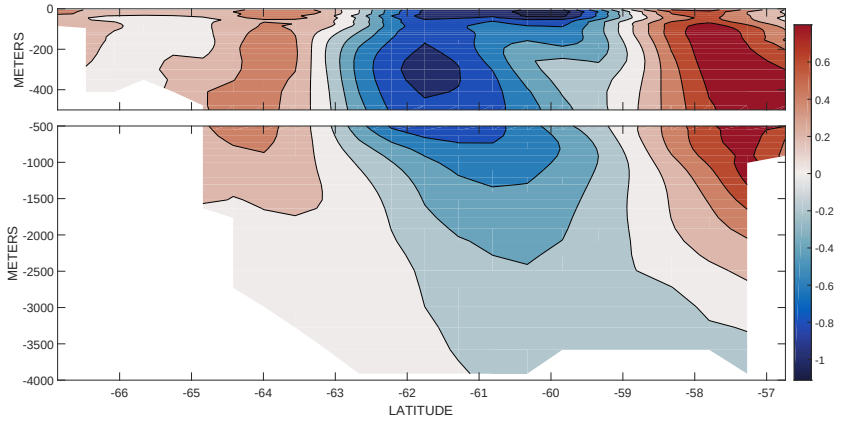

FIG. 21. Anomaly of the zonal flow (cm/s) in the Drake Passage in 1995. Velocity as an annual average in this location proves very stable.

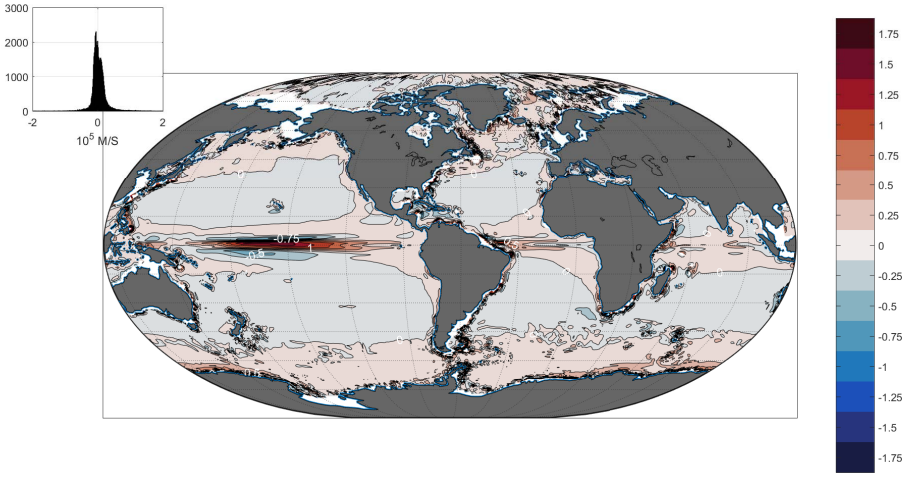

FIG. 22. Twenty-year average vertical velocity ($10^5 w$) (m/s) at 105m depth. This level is an approximate surrogate for the Ekman pumping velocity. The major gyres and equatorial upwelling are readily visible. See Liang et al., 2017b for additional charts and physical discussion.

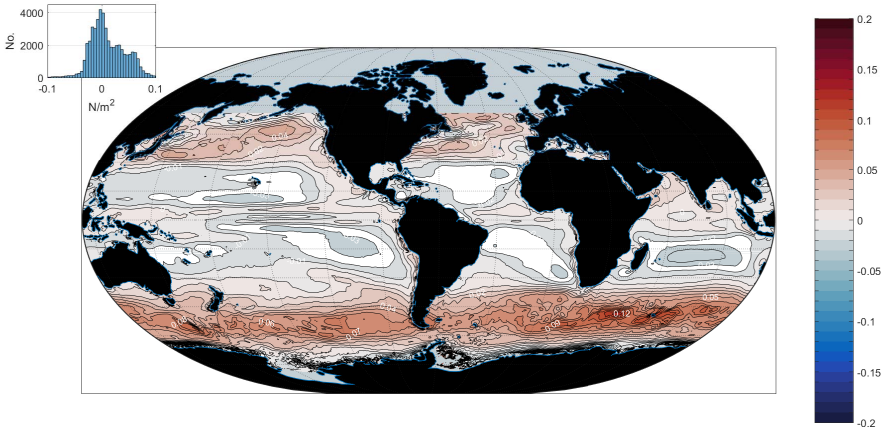

FIG. 23. Adjustments made to the 20-year average zonal windstress, τ_x (N/m^2). This chart can also be interpreted as the average misfit to the ERA-Interim reanalysis. Insert shows the histogram of adjustments, skewed positively.

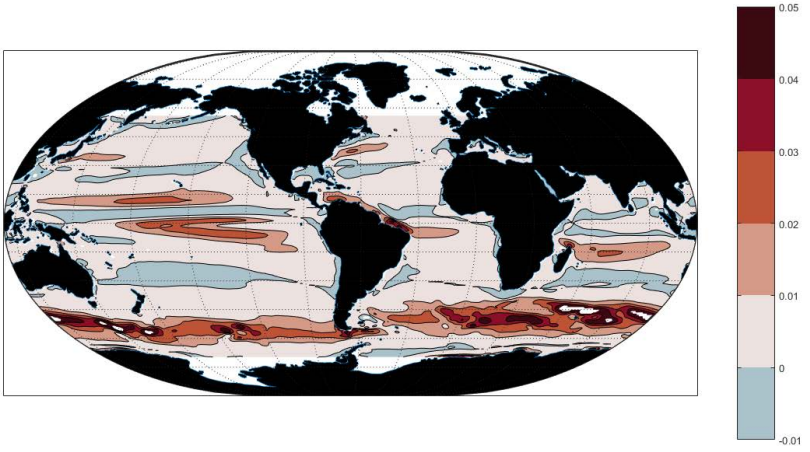

FIG. 24. Rate of working of the mean zonal windstress on the surface circulation (W/m^2). The quantitative importance of the Southern Ocean is apparent.

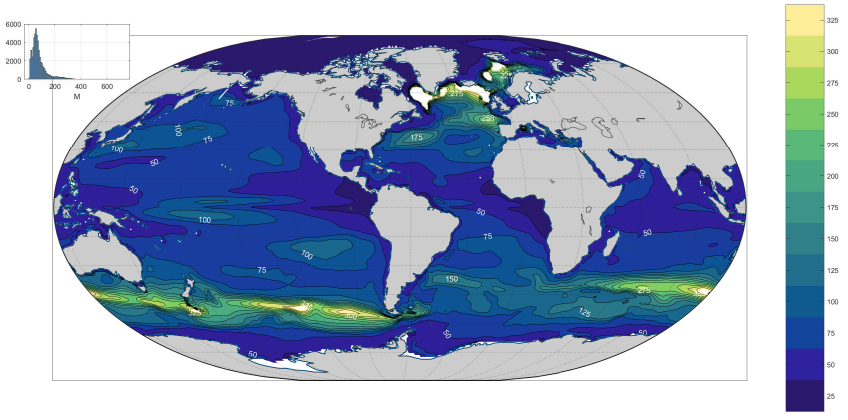

712 FIG. 25. Twenty-year average mixed-layer depth (m) as defined by Kara et al. (2003). Most of the ocean
713 has values near 100m, with extreme values above 700m in the high latitude North Atlantic Ocean and which are
714 truncated here.

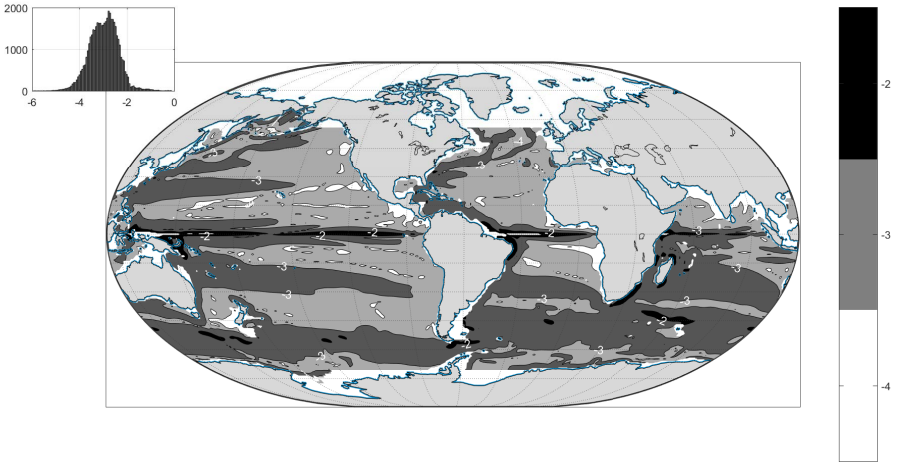

FIG. 26. Logarithm to the base 10 of the estimated Rossby number, based upon a 100km horizontal scale at 722m depth and the 20-year average horizontal speed. Rossby number estimates are a major element in understanding the physics of time-averaged and instantaneous circulations. Numerous other non-dimensional numbers can be computed.

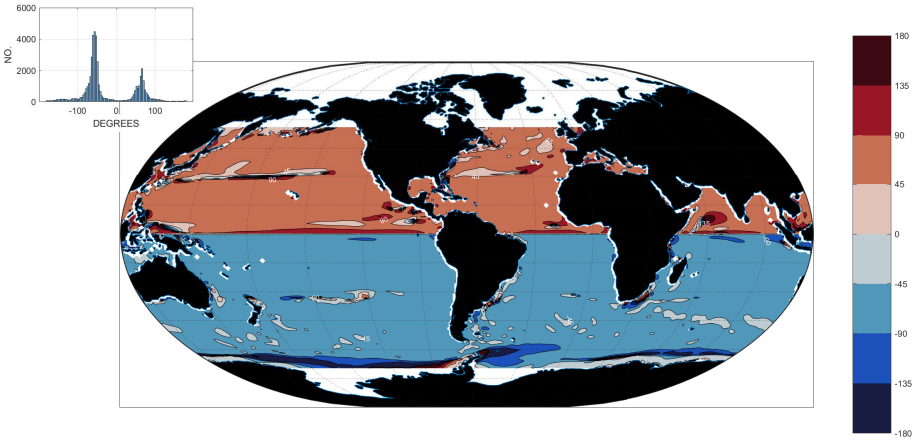

FIG. 27. Angle in degrees between the 20-year average ageostrophic flow at 5m and the 20-year average adjusted windstress. At the sea surface, a perfect Ekman layer would produce $\pm 45^{\circ}$ with the sign changing across the equator. Inset shows the bimodal histogram of angle values. Appearance of a near-classical Ekman layer becomes an important element in any discussion of the global ocean circulation, with many other components determinable from the ocean climatology results (e.g., overall vorticity balance, bottom boundary layer dissipation, et al.).

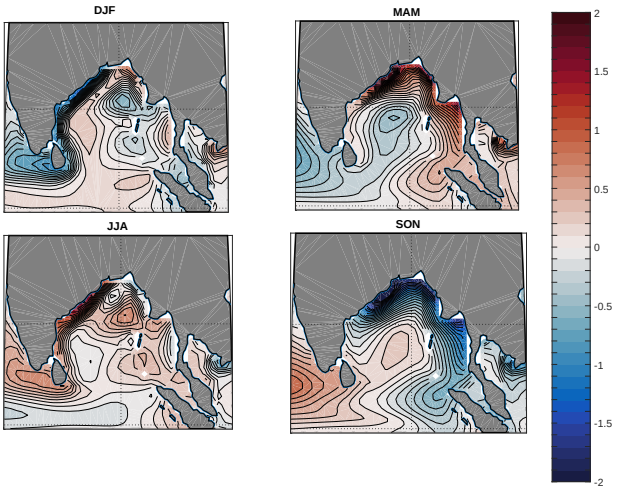

725 FIG. 28. Twenty-year seasonal averages of salinity anomalies at 5m in the Bay of Bengal and which are
726 typical of the regional state estimate characteristics available.